Study of temperature effect on macro-synthetic fiber reinforced concretes by means of Barcelona tests: an approach focused on tunnels assessment

Dimas Alan Strauss Rambo[a,1], Ana Blanco[b], Antonio Domingues de Figueiredo[a], Edson Rodrigo Fernandes dos Santos[c], Romildo Dias Toledo Filho[c] and Otávio da Fonseca Martins Gomes[d,e]

[a] Department of Civil Construction Engineering, USP, Escola Politécnica da Universidade de São Paulo, Rua Professor Almeida Prado 532, São Paulo, 05508-901, Brazil.

[b] Department of Civil and Environmental Engineering, Universitat Politècnica de Catalunya, UPC, Jordi Girona 1-3, 08034, Barcelona, Spain.

[c] Civil Engineering Department, COPPE, Universidade Federal do Rio de Janeiro, P.O. Box 68506, Rio de Janeiro, 21941-972, Brazil.

[d] Centre for Mineral Technology (CETEM), Av. Pedro Calmon, 900, Cidade Universitária, Rio de Janeiro, 21941-908, Brazil.

[e] Postgraduate Program in Geosciences, National Museum, Federal University of Rio de Janeiro, Av. Quinta da Boa Vista, S/N, Bairro Imperial de São Cristóvão, Rio de Janeiro, 20940-040, Brazil.

July, 2017

[1]Corresponding author: e-mail: dimasrambo@gmail.com, Phone: +55(11) 98699-0220.
Present address: Faculty of Technology and Exact Sciences, University São Judas Tadeu, USJT, Rua Taquari 546, CEP 03166-000, São Paulo – SP, Brazil.

Abstract

This paper presents an experimental investigation on the applicability of the Barcelona (BCN) test to evaluate the mechanical properties of a Macro-Synthetic Fiber Reinforced Concrete (MSFRC) submitted to high temperature environments (up to 600°C). BCN tests demonstrated that the MSFRC gradually loses tensile strength an energy consumption density with increasing temperature. Temperatures of 400°C and 570°C shown to be critical to the MSFRC mechanical performance. The residual mechanical behavior of the macro-synthetic fibers was not affected by the temperature up to 100°C. For higher temperatures, the reinforcement showed that may lose part of its crystallinity compromising the MSFRC post-cracking performance. The constitutive model used to determine the stress-strain curves of the MSFRC was capable to reproduce the composite behavior after the event of a fire.

Keyword: Barcelona test; Elevated temperatures; Macro-synthetic fiber reinforced concretes; Tunneling.

Highlights

MSFRC loses residual tensile strength and energy density with rising temperature.

Temperatures of 400°C and 570°C are critical to the MSFRC mechanical performance.

Up to 100°C the residual mechanical behavior of the macro fibers is not affected.

The specimen surface degradation caused by temperature affect BCN test result.

1. Introduction

It is well known that a properly dosed concrete composite reinforced with macro-synthetic fibers (i.e.: MSFRC) may be suitable for structural applications, presenting ductility under compression and great energy absorption capacity under tension [1,2,3,4]. Different from other fiber reinforced composites (e.g.: steel fiber reinforced concretes), the mechanical behavior of a MSFRC is majorly dependent on the frictional bond stablished between the fiber and matrix at the interfacial transition zone [5]. Such characteristic led the macro-synthetic fibers to evolve in terms geometry, anchorage and surface treatment.

In high temperature environments, however, the behavior of a MSFRC is dependent on the thermal gradient established in the element, as well as on the mechanical and physical changes occurred on both: fibers and matrix. This topic represent one of the main unresolved and challenging issues regarding the performance of this composite that still concern the scientific community and the construction sector. The effect of fire exposure and elevated temperatures on the mechanical behavior of a MSFRC is particularly interesting to the case of underground tunnel structures, which frequently employ this type of material.

Once heated, a Portland cement concrete will experience several chemo-physical transformations: release of free and chemically combined water, decomposition of the calcium silicate hydrates (CSH), dehydration of portlandite and decomposition of carbonated phases. As a result, the concrete exhibits reduction of the tensile and compressive strength, cracking, loss of the bond between the aggregates and the cement paste, deterioration of the hardened cement paste and, in some cases, spalling [6]. The addition of micro synthetic fibers (in particular the polypropylene fibers) may reduce the

chance of concrete spalling [7] while macro fibers (e.g. steel, polypropylene), may guarantee residual load-bearing capacity of the structure [8].

Such load-bearing capacity will depend on the type of fibers used, but certainly it will contribute to reducing the risk of a tunnel collapse. This aspect is particularly relevant considering the high costs associated to the reconstruction or repairing of a collapsed tunnel [9,10] and the historic sequence of catastrophic events occurred in such structures submitted to fire loading [9].

Table 1 presents relevant data of previous studies on the effects of high temperature on FRC, including the used type of fiber, the temperatures reached and the tests performed. The notation used to distinguish the material of the fiber is: C for carbon, S for steel, PP for polypropylene and PE for polyethylene. The symbol + is applied for hybrid reinforcement (when more than one type of fiber is used in one mix).

Reference	**Fiber**	**Temperature (^{0} C)**	**Specimen (mm)**	**Tests**
Chen and Liu [11]	C, S, PP, C+S, C+PP, S+PP	200, 400, 600, 800	100 x 100 x 100	Compression and splitting
Peng et al. [12]	S + PP	400, 600, 800	100 x 100 x 100 300 x 100 x 100	Compression Bending and explosive spalling
Sukontasukkul et al. [8]	S, PP, PE	400, 600, 800	350 x 100 x 100	Bending
Colombo et al. [13]	S	200, 400, 600, 800	500 x 75 x 60	Bending
Choumanidis et al. [14]	S, PP, S+PP	280	150 x Ø150	Barcelona test

*C=Carbon; PP=Polypropylene; S=Steel; PE=Polyethylene.

Table 1 - Summary of previous studies on the effect of temperature on FRC

The data presented in Table 1 reveals that previous studies focus on the evaluation of the mechanical properties such as residual strengths or toughness indexes. However, the microstructure of matrix and the damage suffered by the fiber, which are relevant parameters to understand the composite mechanical behavior at high temperatures, are not evaluated.

This paper presents a comprehensive study of the effects of high temperature on MSFRC: from the mechanical performance to the microstructure point of view. The goal was to

establish the pattern of the degradation of the specimen along its central axis and, then, correlate it with the loss of mechanical strength.

The integrated analysis of the mechanical behavior with the characterization of the damage that occurred in the microstructure provide a unique and novel insight into the effects of high temperatures on the performance of MSFRC. Furthermore, the study also sheds light into the applicability of the Barcelona test to evaluate the post-heating residual strength of the material. In fact, this test is one of the few in the literature that can be performed on FRC specimens drilled from real structures that have been exposed to a fire.

2. Experimental campaign

The experimental campaign begins with the manufacturing and curing process employed to the studied MSFRC. Mechanical tests were performed to assess the composite behavior before and after heating. The MSFRC was evaluated with respect to the residual tensile strength through the Barcelona test [15]. Pre and post heating compressive strength and elastic modulus, were also determined. These evaluations provide conditions to assess the influence of temperature on the behavior of the composite. In order to obtain a better understanding of the effect of the temperature variation in the materials structure, tests were performed to characterize the materials structures. The integrity of the fibers before and after heat treatment was evaluated through direct tensile tests and Differential Scanning Calorimetry (DSC). The fiber-matrix interfaces were assessed in all target temperatures by means of a Scanning Electron Microscope (SEM). Such isolated investigations (pre and post heating), represent key points while studying the residual performance of a real structure. Finally, a well detailed explanation is given about the materials characterization, which involves SEM, thermogravimetry (TG), differential scanning calorimetry (DSC) and XRD analysis applied for both: MSRFC, paste and macro-synthetic fibers.

2.1 MSFRC manufacturing and curing

The concrete used in this research was developed using the same materials and mix-design specified to the concrete matrix used to produce the tunnel segments of the "Metro Line 6" under construction in the city of São Paulo, Brazil. The matrix was designed with a High Early Strength Portland Cement (CP V - ARI RS), silica fume, two coarse aggregates (d_{max}:19 mm and d_{max}:9.5 mm), artificial (d_{max}:4.8 mm) and river sand (d_{max}:2 mm) and a polycarboxylate-based superplasticizer (ADVA 525, Grace Company). The matrix composition is summarized in Table 2.

Constituent	**MSFRC**
Portland cement (kg/m³)	400
Granite coarse aggregate d_{max}:19mm (kg/m³)	770
Granite coarse aggregate d_{max}:9.5mm (kg/m³)	330
River sand (kg/m³)	403
Artificial sand (kg/m³)	269
Silica fume (kg/m³)	22
Water (kg/m³)	165
Water/cementitious material ratio	0.39
Superplasticizer (l/m³)	2.75
Micro-synthetic fiber (kg/m³)	0.8
Macro-synthetic fiber (kg/m³)	8

Table 2 - Summary of the MSFRC composition.

The concrete matrix was reinforced with macro-synthetic fibers (BarChip48) commercialized in Brazil by the EPC Group (Elasto Plastic Concrete) specifically for this study. The real tunnel has adopted steel fibers combined with conventional reinforcement to produce the pre-cast segments. Polypropylene micro-fibers, from the Brazilian company Neomatex, were also employed in the mixture in order to inhibit explosive spalling at elevated temperatures respecting the segments specification. The dosage and

properties (supplied by the manufacturers) of both synthetic fibers can be found, respectively, in Table 2 and Table 3.

Macro-synthetic fiber (reinforcement)*	
Specific gravity	0.90 – 0.92
Tensile strength (MPa)	640
Fibers/kg	59500
Youngs Modulus (GPa)	10
Melting point (°C)	159 – 179
Ignition Point (°C)	> 450
Fiber length (mm)	48
Polypropylene micro-fiber (anti-spalling)*	
Density (g/cm³)	0.91
Fibers/kg	130 millions
Melting point (°C)	165
Fiber diameter (mm)	30 μm
Fiber length (mm)	12

*Data provided by the manufacturers

Table 3 – Properties of the used synthetic fibers.

Preliminary tests were carried out in order to define the reference matrix with the desired macro fiber content (8kg/m³) and slump value (~ 8cm). The composite was prepared in a conventional concrete mixer (300 l capacity) at a room temperature of 24°C ± 1°C. First, all aggregates were homogenized by dry mixing for 60s prior to the addition of cementitious materials (+60s of dry mixing). Water and superplasticizer were then slowly added to the mixture, which was subsequently blended for 8 minutes. Both fibers were manually incorporated into the mixture (+ 5 minutes of blending). The concrete mixture was cast in the steel molds 150 x 300 mm (diameter x height) in two equal layers. The concrete consolidation was carried out through a vibratory table (60 Hz) during 30s.

The MSFRC was cured in a wide electric oven at 40°C during 24 h before demolding. Before heating process, the specimens were sealed using a PVC film. After thermal cure, cylinders were cut into two equal pieces (half of the height) in order to generated specimens of 150 x 150 mm (diameter x height) for the BCN test as well as prescribed by the standard UNE 83504:2004 [16]. The specimens were then regularized and keep in dry condition (sealed in plastic bags) for 28 days. Those conditions were the closest possible to the segments production. In addition, 75 x 150 mm (diameter x height) cylinders were extracted from the aforementioned specimens in order to determine the composite compressive strength and elastic modulus.

2.2 Mechanical tests

2.2.1 Barcelona tests

The BCN specimens were submitted to indirect tension following the specification prescribed on UNE 83515:2010 [15]. During the tests, the composites were subjected to double punch test by means of two cylindrical steel punches centered on both upper and bottom surfaces of the specimens (see Figure 1). The ratio between the specimen diameter and the punch diameter was kept in 1:4, while the ratio between their respective heights was 1:5. The total circumferential opening displacement (TCOD) values, were measured at the middle height of the BCN specimens using a chain apparatus, connected to a clip-gauge (Shimadzu Company) with a maximum range of 5mm, instead of the 10 mm required by UNE 83515 [15]. Thus, the residual strength and toughness values remained restricted to a maximum TCOD of 4 mm.

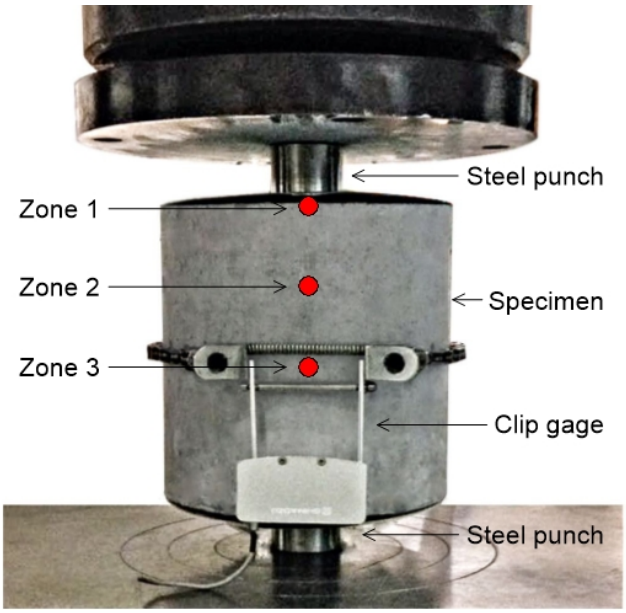

(Single column fitting image; preference for color: online only)

Figure 1 – Set-up of the BCN test and reference zones along the specimen central axis, used for chemical and microstructural analysis.

The tensile strength of the produced MSFRCs was determined through the formulation proposed by Blanco [17], which is analytically derived from the results of the test and provides a σ-ε relation that is valid for the linear-elastic and post-cracking stages. The formulation to estimate the tensile stresses (σ), shown in Eq. (1), is based on the balance of forces interacting in the specimen. The strain (ε) in the linear-elastic stage is obtained as the tensile stress to the modulus of elasticity (E) ratio. After the cracking, Eq. (2) is used to estimate the strain. This expression was derived using the principle of the virtual works.

$$\sigma = \frac{F_P}{2 \cdot \pi \cdot A} \cdot \frac{cos\,\beta - \mu_k \cdot sen\,\beta}{sen\,\beta + \mu_k \cdot cos\,\beta} \quad with\ A = \frac{d \cdot h}{4} - \frac{d'^2}{4 \cdot tan\,\beta} \qquad \text{(Eq.1)}$$

$$\varepsilon = \frac{n\delta_P}{\pi R} \cdot \tan\beta \cdot \sin\left(\frac{\pi}{n}\right) \qquad \text{(Eq. 2)}$$

In Eq. (1) and Eq. (2), several variables are involved: the load applied during the test (F_P), the failure angle of the material (β), the kinetic friction coefficient (μ_k), the diameter and height of the specimen (d and h), the diameter of the steel punch where the load is applied (d'), the number of cracks (n), the radius of the specimen (R) and the displacement registered during the test (δ_P). Most of these parameters are directly obtained from the results of the test (F_P and δ_P), the geometrical characteristics of the specimen (d = 150 mm, h = 150 mm and R = 75 mm) or the test setup (d' = 37.5 mm). The failure angle β is determined from the conical wedge formed during the test under the steel punches according to Eq. (3), where φ is the internal friction angle of the material (this angle determines the cracking surface of the conical wedge as shown in Figure 2). The actual length of the conical wedge (l), and the consequent angle β, was measured for several specimens tested after the thermal treatment up to 25°C, 200°C, 400°C and 600°C (see item 3.2).

$$l = \frac{d'}{2} \cdot tan\varphi \qquad \text{(Eq. 3)}$$

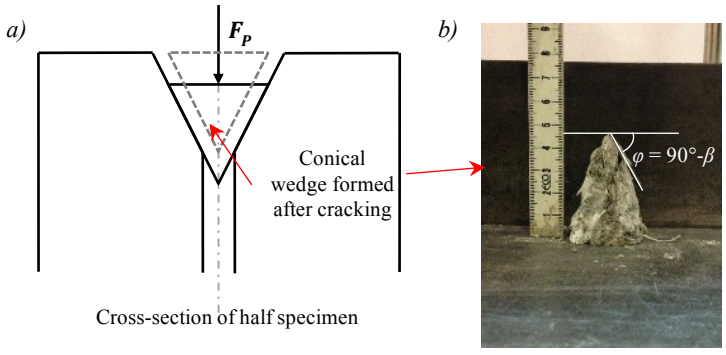

(1.5 column fitting image; preference for color: online only)

Figure 2 - (a) Cross-section of half specimen after cracking and formation of the cone and (b) conical wedge from specimen with thermal treatment up to 200°C.

196 The kinetic friction coefficient (μ_k) of the concrete is a parameter that has not been studied
197 in detail in the literature. In fact, the information available refers to the static friction
198 coefficient of concrete (μ_s), however it is known that μ_k should be smaller than μ_s for the
199 same surface. This is particularly true for the case of the Barcelona test since two concrete
200 surfaces are subjected to a significant relative displacement. In the absence of reliable
201 values of μ_k, a reasonable approximation is 0.7, which corresponds to the limit value
202 between smooth and rough surfaces defined in the Model Code 2010 [18].

203 In order to assess the post-heating tensile behavior of the studied MSFRC, BCN
204 specimens were heated in an electric oven (Inforgel Company) up to the following
205 temperatures: 200°C, 400°C, and 600°C. Experiments on control specimens (unheated
206 MSFRCs, just cured at 40°C) were also carried out. The BCN specimens were covered
207 by steel mesh in order to avoid damage to the furnace in case of explosive spalling. The
208 heating rate was maintained in 16°C/min (largest value allowed by the used furnace).
209 Differently from a real tunnel fire (single-face heating), inside the oven, heating occurs
210 in the entire outer surface of the specimens. Seeking to stabilize the specimens at the
211 studied target temperatures, a sustained thermal load of 60 min was employed. The choice
212 for this exposure time is based on data about duration of fires (along the last 5 decades)
213 reported by the International Tunneling Association (ITA) [19]. After the heating process,
214 the cylindrical specimens destined to the residual BCN tests were cooled down naturally
215 within the furnace until reach the room temperature. Such process was carried out to
216 prevent large thermal gradients capable of cracking the concrete composite. At the end of
217 the test, the following parameters were determined: First crack tensile strength (σ_{cr}),
218 residual tensile strengths for strains of 0.2% ($\sigma_{0,2\%}$) and 0.4% ($\sigma_{0,4\%}$), and energy density
219 for strains of 0.2% ($A_{0,2\%}$) and 0.4% ($A_{0,4\%}$).

220 **2.2.2 Compressive strength and elastic modulus**

The compressive strength (f_c) and elastic modulus (E_c) of the produced MSFRC were carried out in 75 x 150mm (diameter x height) cylinders using three specimens for each target temperature (see item 2.1). As well as in the BCN test, compressive strength assessment was performed not only at room temperature (25°C) but also in specimens heated up to 200°C, 400°C and 600°C. The compressive load was applied at a rate of 0.1mm/min by using a Shimadzu universal testing machine (model UH-F1000kN) with a computer-controlled hydraulic servo system. The composite axial strain was determined by the average of two displacement transducers attached around the specimen. The elastic modulus was obtained on the elastic range of the stress-strain curves located between 0.5 MPa and $0.3f_c$.

2.2.3 Direct tensile tests of macro-synthetic fibers

Monotonic tension tests were performed in single macro-synthetic fibers in order to evaluate their mechanical properties at room temperature, as well as, to assess the effect of temperature on the fibers residual tensile properties. In that sense, fibers with 10 mm of gage length were tensioned in a horizontal electromechanical testing machine (MTS, model Tytron 250) coupled to a 50 N load cell and a 5μm precision extensometer. Load and displacement measurements were recorder at a rate of 4 Hz. The test methodology adopted here follows the study proposed by Estrada et al. [21] for the evaluation of fibers already cut in the length of use. The results obtained in such condition may differ in terms of strength and, in particular, modulus of elasticity, with relation to the tensile test performed on original yarns usually employed by the producers of fibers. However, it allows to evaluate the fiber performance as a function of temperature, which is one of the key objectives in the present study. A displacement rate of 0.4 mm was adopted to all direct tensile test. For each studied temperatures, 6 macro-synthetic fibers were tested. Each single fiber was glued to a paper template in order to allow a perfect alignment with

246 the machine grips. The ultimate tensile strength (σ_{UTS}) of fibers was calculated dividing
247 the maximum load value by the fiber cross-sectional area obtained in the fracture site.
248 The fracture planes of the fibers were analyzed through a Scanning Electron Microscope
249 (SEM) Hitachi TM3000 and subsequently treated using the software ImageJ. The elastic
250 modulus was calculated in the ascending branch of the stress-strain curves located
251 between 10% and 40% of σ_{UTS}. The obtained data were also analyzed through analysis of
252 variances (ANOVA).

253 **2.2.4 Materials characterization**

254 **2.2.4.1 Matrix and fiber-matrix interfaces (SEM, TG, DSC)**

255 The fiber-matrix interfaces of the thermal treated MSFRC (25°C, 200°C, 400°C and
256 600°C) were investigated in three different zones along the central axis of the BCN
257 specimens: 0 (Zone 1), 3.75 (Zone 2) and 7.5cm (Zone 3) (see Figure 1). The Scanning
258 Electron Microscope (SEM) was operated using 25 kV of acceleration tension and 30 mm
259 of working distance. The samples (extracted from the fractured BCN specimens) were
260 attached to a circular plate-shaped stage (diam: 20 mm) and analyzed without any coating.
261 Thermo Gravimetric (TG) analyses were carried out at the Zone 3, using pulverized
262 sample material (~ 40 mg) obtained from the already tested BCN specimens. To extract
263 the powder a rotary impact drill was employed. The samples were heated in platinum
264 sample holders from 35°C to 1000°C in a TA Instruments, SDT Q600 model
265 TGA/DTA/DSC simultaneous apparatus at a heating rate of 10°C min^{-1} and using 100
266 mL/min of nitrogen flow. An isothermal step of 60 min at 35°C was carried out before
267 performing TG analysis. Such process was conducted in order to eliminate the residual
268 non-bonded free water present in the powder material. X-ray diffraction (XRD) analyses
269 were also carried out in the Zone 3 of the thermal treated BCN specimens. The samples
270 used in the XRD analyses were also obtained from the powder extracted by the impact

drill. Operating conditions for qualitative analysis of the Bruker D8 advance instrument were set to 40 kV and 40 mA using CuK$\alpha_{1,2}$ radiation. XRD profiles were recorded in an angular range 2θ of 13° to 60° with increments of 0.02°. The choice of qualitative analyzes was based on the intense quartz peaks (aggregate phase) present in the MSFRC diffractograms, as well as the difficulty of maintaining the material proportions (i.e: aggregates and paste) in the collected samples. Since the intense quartz peaks present on the diffractograms of the MSFRC, can hinder the identification of compounds with minor peaks, TG and XRD analysis were also carried out in samples prepared from the cement and from the paste.

2.2.4.2 Macro-synthetic fiber (crystallinity degree)

In general, polymers are composed by amorphous phases. However, as the fibers are produced by extrusion and stretching, they could present a higher level of crystallinity. Their mechanical properties, directly depends on the crystalline phase which, in turn, is related with the packaging of the chains in an organized manner [20,21]. Once the crystalline phase is affected by thermal loads, an investigation on the degree of crystallinity of the employed macro-synthetic fibers (polypropylene) was developed. The goal, therefore, was to correlate the losses of the crystallinity of fibers with the decrease of the MSFRCs tensile performance when exposed to heat. The crystallinity percentage was determined by using the area under the peak relative to the melting of the crystalline phase obtained by DSC, as well as shown in the Equation 4.

$$\%X_c = \frac{\Delta H^0_{sample}}{\Delta H^0_{standart}}\ x\ 100 \qquad \text{(Eq.4)}$$

Where:

$\%X_c$ = crystallinity percentage

ΔH^0_{sample} = sample melting enthalpy

$\Delta H^0_{standart}$ = enthalpy of the reference sample (209J/g) [22]

TG/DSC analyses were carried using fragments of fibers (10mg) extracted manually from the tested BCN specimens. The fiber samples were heated in platinum sample holders from 25°C to 700°C in a TA Instruments (STA6000) model Perkin Elmer TGA/DSC simultaneous apparatus at a heating rate of 20°C min^{-1} and using 20 mL/min of nitrogen flow. An isothermal step of 1 min at 25°C was carried out before performing DSC analysis. To ensure no cement and aggregate contamination, the samples were soaked in 1 $mol.L^{-1}$ hydrochloric acid solution (at 40°C) and stirred for about 30 minutes.

3. Results and discussion

In this item, the mechanical performance and microstructural features of the MSFRC, before and after exposure to the target temperatures, (200°C, 400°C and 600°C), were carefully examined. The obtained data (e.g.: tensile and compression strength, elastic modulus, etc) were treated through analysis of variances (ANOVA). As shown in Figure 3, no explosive spalling was observed in the composites after the heating program. From 200°C and above, however, all specimens presented thermal cracking and fiber detachment.

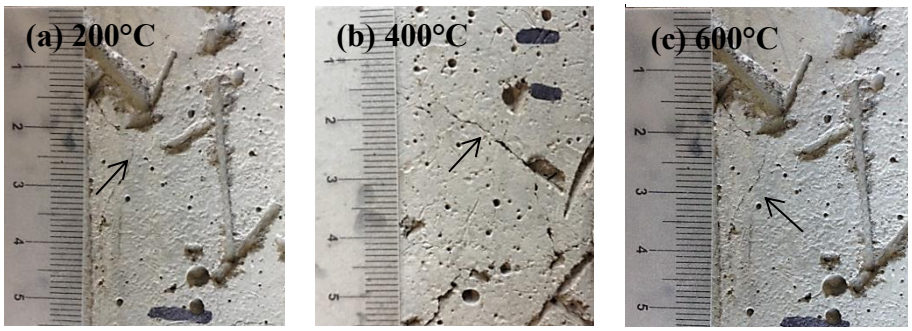

(1.5 column fitting image; preference for color: online only)

Figure 3 – Surface degradation observed on the BCN specimens after thermal treatment up to (a) 200°C, (b) 400°C and (c) 600°C.

3.1 Effect of temperature on the MSFRC compressive strength and elastic modulus

Figure 4 presents the variation of compressive strength and elastic modulus evolution of the MSFRC (at an age of 28 days) for each tested specific target temperature (25°C, 200°C, 400°C and 600°C). The average results can be found on Table 4. The specimens tested at room temperature presented an average compressive strength of 58.2 MPa as well as an elastic modulus of 28.1 GPa.

The residual compressive strength values obtained at 200°C, 400°C and 600°C, shown to be, respectively, 9.2%, 34.6%, 64.9% lower than the value reached at room temperature. The losses in the elastic modulus were still greater for the same target temperatures, 31.0%, 87.6% and 96.6%, respectively. As can be seen in Figure 4b, the most pronounced decrease in the modulus of elasticity occurs between 200°C and 400°C and represents a reduction of 82.1%. This is in line with other studies that also identify the range of 200°C-400°C as the one presenting the main difference between the material responses in most cases [11,13].

This continuous loss of strength is given by different processes, among which can be highlighted, the dehydration of hydrated products present in the concrete matrix, the mismatch between the aggregate and the cement paste thermal expansion, the increases in the matrix and aggregate porosity and the degradation of synthetic fibers. These processes will be further addressed in the item 3.4 and correlated with microstructural analyses.

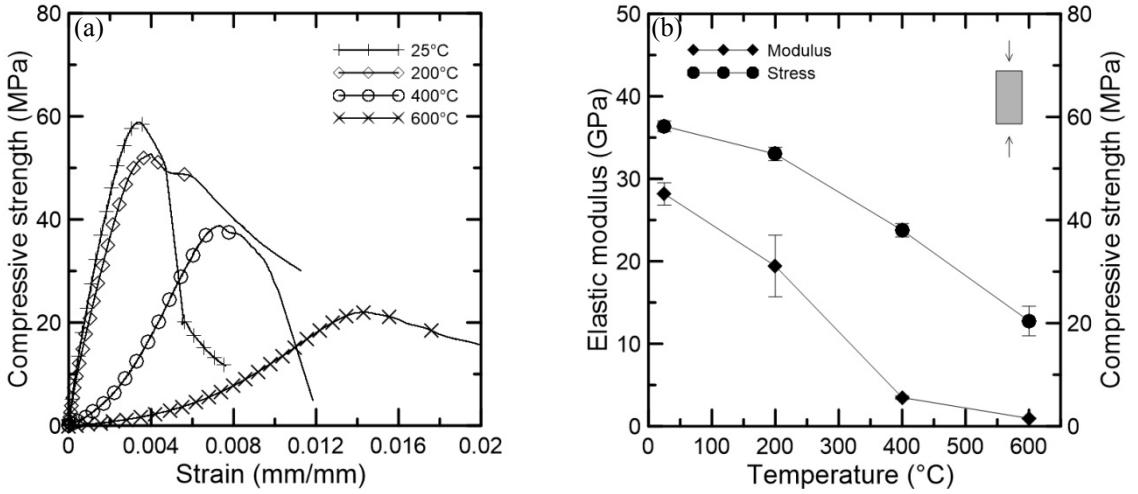

(1.5 column fitting image; grayscale)

Figure 4 – (a) Typical stress-strain curves obtained for the MSFRC under compression before and after heat treatment; (b) Average loss in compressive strength and elastic modulus obtained for each studied temperature.

Target temperature	Compressive strength		Tensile strength (BCN)		
	f_c (MPa)	E_c (GPa)	σ_{cr} (MPa)	$\sigma_{0.2\%}$ (MPa)	$\sigma_{0.4\%}$ (MPa)
25°C*	58.20 (1.03)	28.17 (1.35)	4.10 (0.16)	2.42 (0.15)	1.90 (0.13)
200°C	52.82 (1.30)	19.43 (3.73)	3.56 (0.15)	2.40 (0.15)	1.87 (0.11)
400°C	38.02 (1.31)	3.48 (0.21)	3.28 (0.17)	1.11 (0.17)	-
600°C	20.42 (2.86)	0.95 (0.09)	1.53 (0.10)	1.31 (0.11)	-

*Room temperature.

Table 4 – Post-heating mechanical strength obtained for the MSFRC. Standard deviation values are presented in parentheses.

3.2 Effect of temperature on the MSFRC post-heating tensile strength

As reported in the item 2.2.1 the length of the conical wedge (*l*) was measured for all target temperatures in order to obtain the angle β, necessary to tensile strength

349 determination. The β values obtained for 25°C, 200°C, 400°C and 600° were,
350 respectively, 21°, 22°, 18° and 18°. Given the difficulty associated with the extraction of
351 a representative number of cones from the BCN specimens, especially in the case of well
352 degraded concretes (heated up to 400°C and above), the authors chose to employ an
353 average angle β of 21° for the calculation (common to all temperatures). In all studied
354 temperatures, the tensile behavior of the MSFRCs was expressed in the form of stress
355 *versus* strain curves (see Figure 5). All composites presented strain softening behavior
356 when submitted to the BCN test, even those tested at room temperature. Through Figure
357 5 is possible to percept that the MSFRC crack strength (σ_{cr}) decreases gradually with
358 increasing temperature, being the referred decrease more pronounced between 400 and
359 600°C. Figure 6a presents the average values σ_{cr} for all MSFRCs. The average first crack
360 strength values obtained for 200°C, 400°C and 600°C were, respectively, 13.2%, 20%
361 and 62.5% lower than that obtained for 25°C.

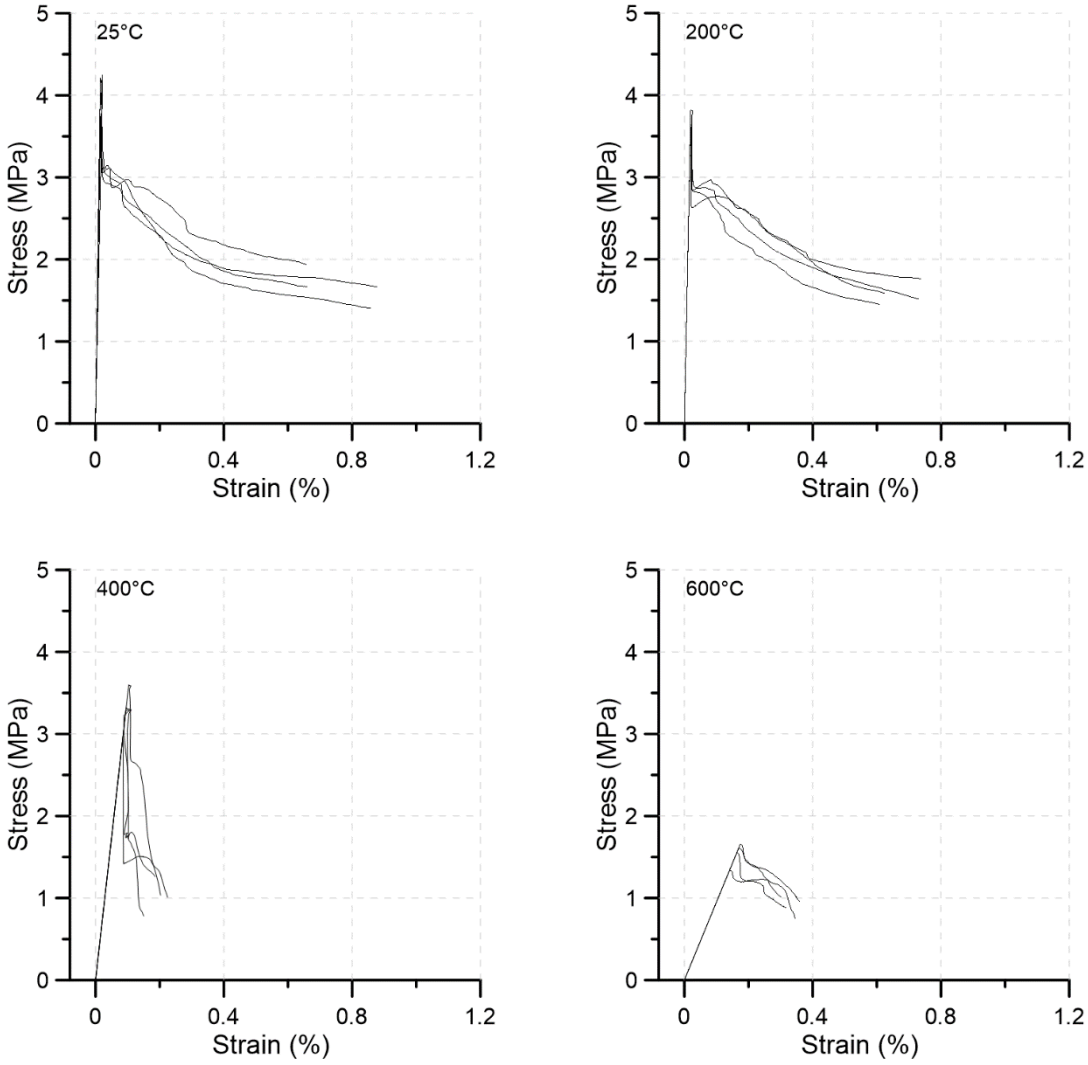

(1.5 column fitting image; grayscale)

Figure 5 – Stress-strain curves obtained from the results of the Barcelona test for the MSFRC specimens submitted to different temperatures.

The post-cracking response of the MSFRCs varies significantly depending on the temperature. According to the curves in Figure 5, the MSFRC exposed up to 200°C maintain similar values of the residual strength and overall ductility when compared to the MSFRC at room temperature. However, from 400°C upwards, the bearing capacity of the material is significantly reduced (see item 3.4). Figure 6a shows the residual strengths of all MSFRCs, associated to strain levels of 0.2% and 0.4%.

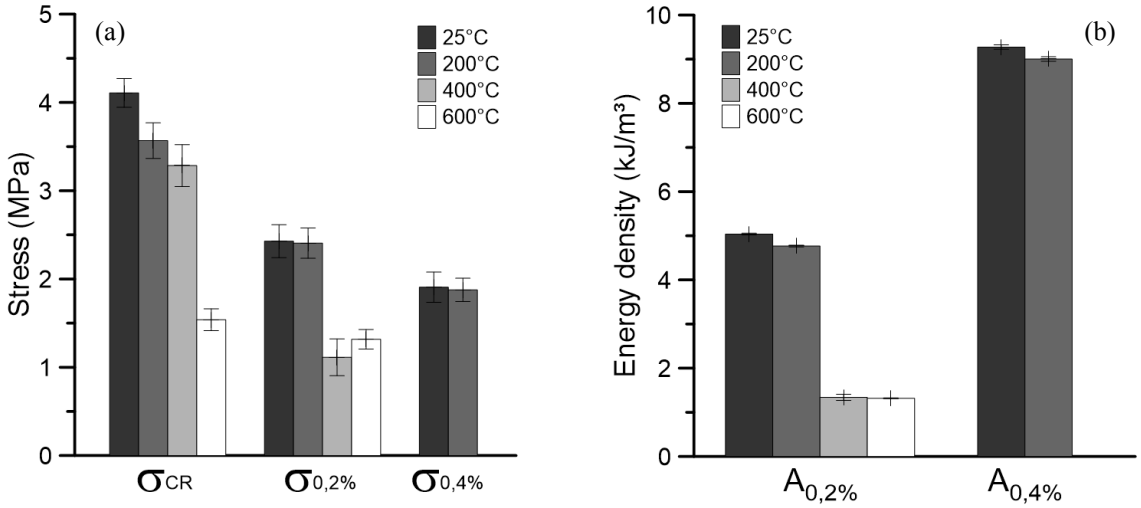

(1.5 column fitting image; grayscale)

Figure 6 – (a) Average first crack tensile strength and residual strengths for strains of 0.2% and 0.4%, and (b) energy consumption density for strains of 0.2% and 0.4%.

The average $\sigma_{0.2\%}$ obtained for 200°C, 400°C and 600°C were, respectively, 0.9%, 54.2% and 45.7% lower than that obtained for 25°C. Such outcome may be explained by the decomposition process suffered by the fibers when subjected to high temperatures, which already starts at about ~300°C (Figure 7).

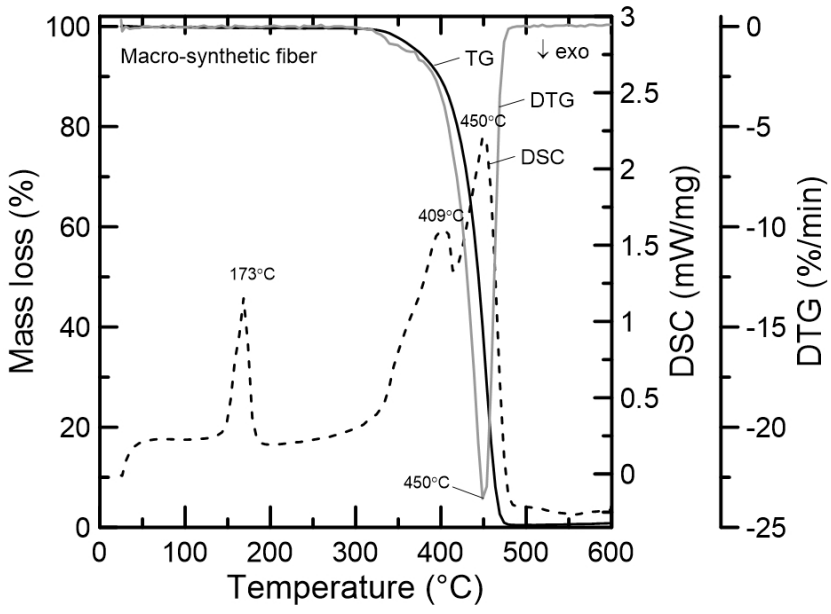

(Single column fitting image; grayscale)

Figure 7 - DSC, TG, and DTG of the macro-synthetic fibers.

The average $\sigma_{0.4\%}$ obtained for 200°C was only 1.6% lower than that measured for 25°C, thus indicating that the fibers exposed to such temperature are still capable of providing ductility to the composite. The MSFRCs specimens exposed to 400°C and 600°C did not reach that level of strain during the test (see Figure 5).

Figure 6b presents the values of energy consumption density (in kJ/m^3) associated to the aforementioned strain levels. This parameter is calculated as the average area below the stress-strain curves of all specimens. It has been used in previous studies [23,24] to assess the overall post-cracking response of fiber reinforced concrete instead of only using specific values of residual strength. The results also confirm that the critical temperature which alters the response of the MSFRC is 400°C. The average energy consumption densities at a value of strain of 0.2% for 200°C, 400°C and 600°C were, respectively, 5.4%, 73.4% and 89.9% lower than that obtained for 25°C. The same analysis for a strain of 0.4% is only possible for the MSFRC exposed to 200°C and its value is only 2.9% lower than that corresponding to the reference temperature (25°C). As well as the compression results, the effect of temperature on the MSFRCs will be further addressed in the item 3.4, in which the mechanical results are linked to the microstructural analyses.

3.3 Effect of temperature on the tensile strength and elastic modulus of the macro-synthetic fibers.

Based on the procedure described in the item 2.2.3, the residual tensile strength and elastic modulus of the studied macro-synthetic fibers, were determined for 25°C, 75°C and 100°C. Regarding tensile strength, the average values obtained for the aforementioned temperatures were respectively 275 MPa, 289 MPa and 325 MPa. With relation to the

elastic modulus, the obtained average values were 2.6 GPa, 2.6 GPa and 2.9 GPa for the same temperatures. For temperatures above 100°C, longitudinal shrinkage was observed along the fiber length, impairing the test from the execution point of view. As reported before, six fibers were tested for each studied temperature. The obtained results showed that the low temperatures employed for the residual tensile tests (below the melting point) were not capable to alter the fiber mechanical properties (see Figure 8). Such uniformity was clearly noticed comparing the strength and elastic modulus of all fibers in statistical tests, in which the p-values were higher than 0.05 (ANOVA).

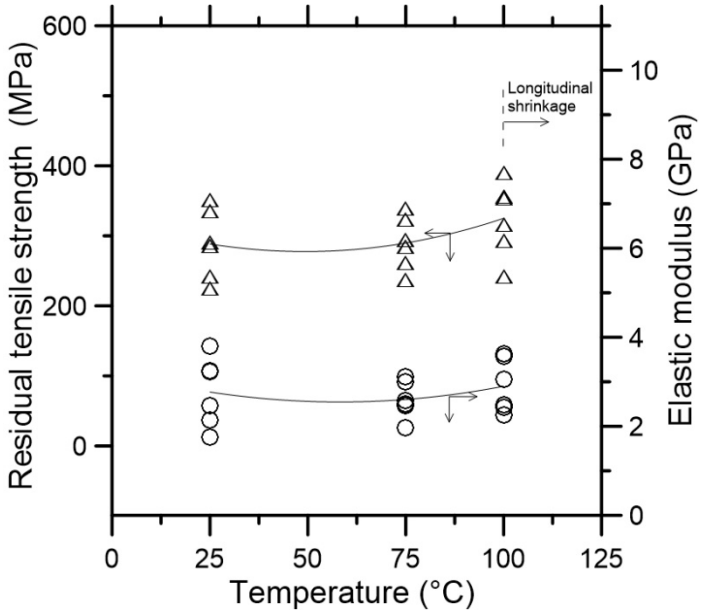

(Single column fitting image; grayscale)

Figure 8 – Effect of temperature on the tensile strength (a) and elastic modulus (b) of the studied macro-synthetic fibers.

3.4 Micro-structural characterization and mechanical properties

Figure 9 presents the TG and DTG curves obtained for the MSFRC, in all studied target temperatures. These curves refer to the central portion of concrete located at Zone 3 (7.5cm from the top). The TG and DTG curves are plotted starting from the end of the aforementioned isothermal stage at 35°C (see item 2.2.4.1). Initially, in the reference sample (25°C_Zone 3) the imposed heating regime tends to drive out the free water (present in the matrix) and accelerate its diffusion through the hardened paste. In parallel, calcium silicate hydrate (CSH) and ettringite (AFt) starts to dehydrate increasing the porosity of cement paste while reducing the strength of the whole composite. Given the overlapping of the DTG peaks, the decomposition process of such compounds cannot be clearly distinguished.

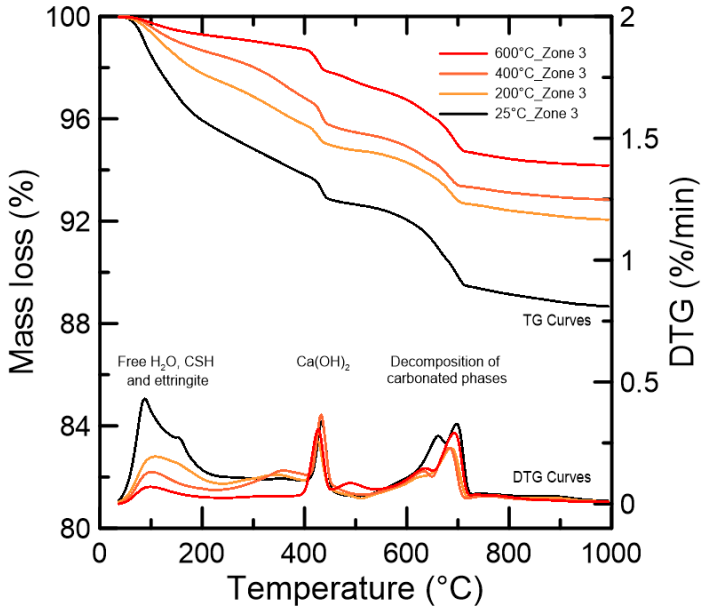

(Single column fitting image; preference for color: online only)

Figure 9 - TG and DTG curves of powder material extracted from the central axis of the MSFRC at room temperature and after heating process up to 200°C, 400°C and 600°C.

The presence of the CSH and AFt was detected by XRD in the diffractograms performed on the MSFRC (25°C_Zone 3) and in the hydrated cement paste (Figure 10). CSH is

formed during the hydration of alite (C_3S) and belite (C_2S) phases. Ettringite, however, is formed from the phases commonly called as aluminate (C_3A) and gypsum ($C\check{S}H_2$), consuming high amount of water [25]. All of these phases (alite, belite, aluminate and gypsum) were detected in the cement powder through the XRD, together with the ferrite phase (C_4AF) (see Figure 10).

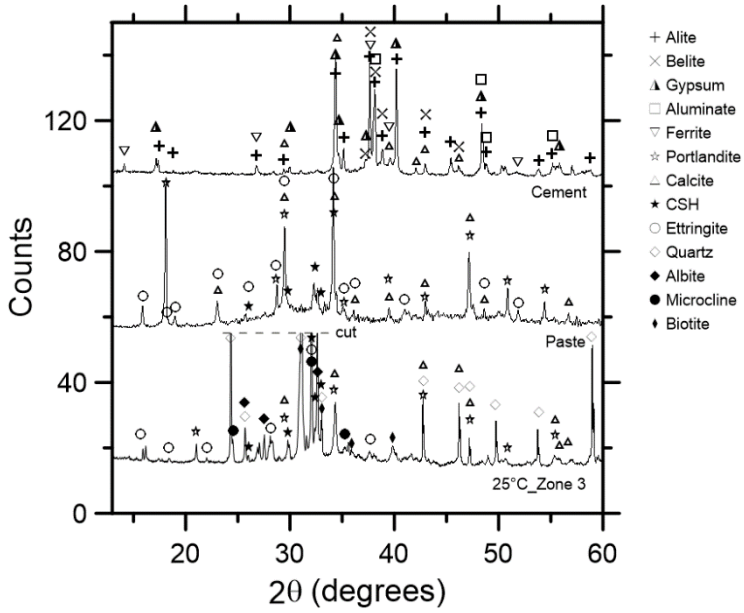

(Single column fitting image; grayscale)

Figure 10 - XRD patterns obtained for the cement, paste and for the MSFRC (25°C_Zone 3).

The first step of dehydration, corresponding to CSH and AFt present a long descending branch which extends to about 500°C (Figure 9). Other degradation steps are still observable on the TG curve of the reference sample (25°C_Zone 3). The second major step, between 400 and 500°C, refers to the dehydration of the calcium hydroxide ($Ca(OH)_2$) [25]. For temperatures above 500°C, it is possible to observe the decomposition of the carbonated phases identified by XRD as calcite ($CaCO_3$).

458 In the Zone 3 of the MSFRC heated up to 200°C, it is possible to percept that only the
459 CSH and AFt were partially decomposed (see first DTG peak on Figure 9). Greater
460 dehydration does not occur because the imposed heating regime is not capable, or long
461 enough, to take the core (Zone 3) up to 200°C. Thus, great part of the microstructure is
462 preserved and so the matrix compressive and tensile strength (see Table 4). As the internal
463 temperature increase, thermal expansion of the aggregates give rise to internal stresses
464 within the composite. Such stress, resulted in micro-cracks, which shown to be visible to
465 naked eye in the studied composites (Figure 3). In the MSFRC heated up to 200°C, no
466 fiber degradation was observed. However, the fibers located close to the specimen surface
467 (Zone 1), presented longitudinal shrinkage. According to Diaz and Youngblood [26],
468 thermal shrinkage is a particular characteristic of highly aligned polypropylene
469 reinforcements, in which values of shrinkage of up to 6% may be expected, depending on
470 the applied restriction and temperature conditions. However, as reported by the same
471 authors, what actually occurs with rising temperature is a joint effect of thermal shrinkage,
472 thermal expansion and creep occurring at the same time in the polymer. SEM images
473 were used to investigate the inner portions of the composite, looking for alterations on
474 the fiber reinforcement. The micrographs, however, did not show any difference between
475 the reinforcement at 25°C and 200°C just below the surface. The thermal field established
476 in a concrete cylinder exposed to elevated temperatures is time-dependent and, for a short
477 exposure time (case of this study), the temperature decreases significantly along the radial
478 direction. In addition, temperature histories of points inside the furnace and on the faces
479 of the heated specimen may present great differences [27]. Studies performed by Shaikh
480 and Vimonsatit [28] where thermocouples were embedded in cylinders exposed to
481 elevated temperatures (heating rate: 8°C/min) revealed that even after 1h at 200°C the
482 central portion of the concrete specimens (distant 5cm from the surface) does not reach

more than 120°C. Such results allow us to presume that for larger specimens (case of BCN specimens) heated up to same temperature (200°C), the thermal gradient till the center is even greater. This may explain why the mechanical behavior at 200°C is so close to that at 25°C (under compression and tension) and why the macro reinforcement remains intact as well as part of the CSH and Aft. Such idea also agree well with the mechanical results reported in the item 2.2.3 which prove that there is no residual strength decrease in the macro reinforcement up to 100°C.

Observing the thermogravimetric analysis for the Zone 3 of the MSFRC heated up to 400°C, it is possible to percept a more intense decomposition of CSH and AFt up to about 250°C. The rest of the curve (above 250°C), as well as in the MSFRC heated up to 200°C, remained practically unchanged. As a result of a more pronounced decomposition of hydrated phases (especially CSH), a loss of 34.6% was observed in the compressive strength (see item 3.1). Regarding the tensile performance of the MSFRC, especially in the post cracking region, great decreases were observed for 400°C and above (Table 4). Such results are directly related to the matrix thermal degradation, but also to the changes in the reinforcement strength (i.e. in the polymer crystallinity). Figure 11 shows micrographs of the interfaces between fibers and matrix at room temperature (Zone 3), and after heating process up to 400°C: (Zone 1, Zone 2 and Zone 3). At room temperature (Figure 11a), both micro and macro-fibers appear intact in the fractured MSFRC. The circular and elliptical hollows observed for 400°C (Zone 1) indicate clearly that, the temperature in this site was capable to fully decompose both polymeric fibers (see Figure 11b).

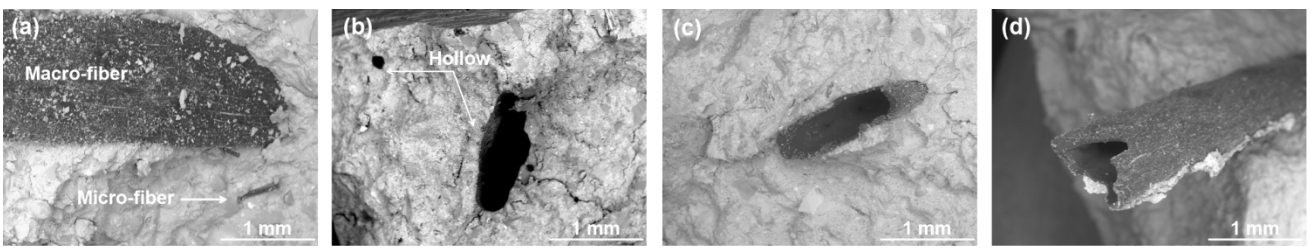

(2 column fitting image; grayscale)

Figure 11 – Interface between the matrix and the macro-synthetic fibers (a) at room temperature and after heating process up to 400°C: (b) Zone 1, (c) Zone 2 and (d) Zone 3.

The absence of fibers was observed up to around 1.6 cm from the border of the specimen, which means that the macro reinforcement was fully compromised in approximately 52% of the specimen volume, while the rest retain part of its functionality. This phenomenon was also observed in concrete composites containing macro-synthetic fibers studied by Choumanidis et al. [14] where BCN specimens were submitted to a low heating ramp (2°C/min) up to 280°C.

The micrographs performed on the MSFRC inner portions (i.e.: Zones 2 and 3), however, shown that, instead of hollows, "polymeric tubes" were formed into the fiber beds at 400°C (Figure 11c-d). Such distinct shape, results from different process associated to the heating regime. First, the polymer expand [29] inside the porous matrix when the temperature get closer to the polymer T_m. Once melted, the portion of polymer which remains in the "fiber bed" (adhered to surrounding matrix) experiences a non-isothermal recrystallization process using the walls as areas of nucleation and growing of crystals (during the cooling process). This will only occur, however, if the temperature is not able to fully decompose the polymer. Observing the micrographs shown in the Figure 11c-d, it is well probable that at least partial polymer decomposition occurred in the Zones 2 and 3 of the MSFRC heated up to 400°C.

As well as the concrete, the polymer loses its strength with increasing temperature up to 400°C. Figure 12 shows the comparison of the melting enthalpy generated by unheated fibers (25°C) and fibers extracted from Zone 3 of the specimens heated up to 400°C. Dividing the measured enthalpies by the enthalpy of the reference sample (209J/g) [22],

crystallinity degrees of 46.7% and 35.1% were observed for the fiber extracted from the reference MSFRC (25°C-Zone 3) and that heated up to 400°C (Zone 3), respectively. This drop on the crystallinity reduces the reinforcement strength [30], which in turn affect the MSFRC post cracking performance (Figure 5). Due to the brittleness presented by the fibers exposed to 400°C (vitreous rupture) it was impossible extract them for tensile strength determination. The absence of fibers in the Zone 1 (up to 1.6cm from the border) and the reduced crystallinity measured for the fibers located in the Zone 3, were responsible by the great decrease in the post-cracking behavior of the MSFRC heated up to 400°C, previously discussed in the item 3.2.

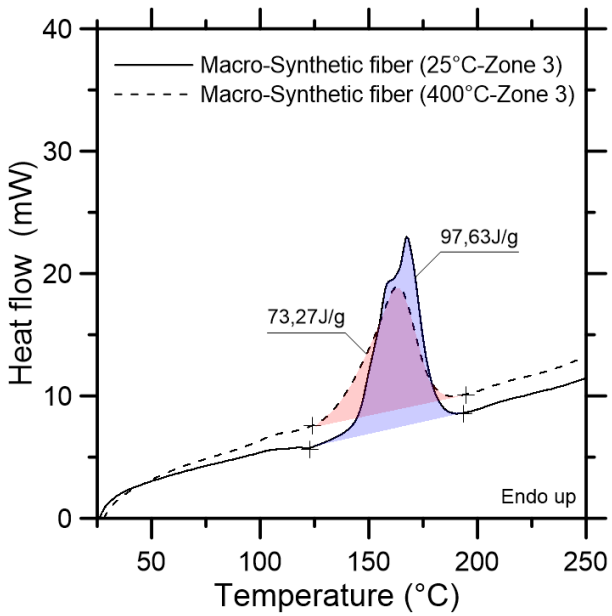

(Single column fitting image; preference for color: online only)

Figure 12 - Melting enthalpy generated by unheated fibers (25°C-Zone 3) and by fibers extracted from Zone 3 of the specimens heated up to 400°C.

Micrographs of the Zones 1, 2 and 3 of the MSFRC heated up to 600°C, revealed the complete absence of fiber reinforcement along the depth of specimens. Such fact indicates that the temperature, even in the Zone 3, exceeded the mark of 300°C (beginning of

548 polypropylene degradation). In addition, the heating regime was long enough to cause
549 fully polymer decomposition. However, it is possible to observe from the
550 thermogravimetric analysis (600°C-Zone 3) that the peak of portlandite, at around 430°C,
551 is still observable (Figure 9). Such observation makes clear that the core reached a
552 temperature very close to 400°C while the external faces were submitted to 600°C. Given
553 the inferences about the thermal gradient experienced by the specimen heated about
554 600°C, the small peak at around 100°C, observed on the DTG analysis, was attributed to
555 a small rehydration process occurred during the powder sampling.
556 At high temperatures, also the aggregates lose their mechanical properties. In this study,
557 granite aggregates were used as the main component in the concrete composition (see
558 Table 2). As a result, great XRD peaks of quartz, albite, microcline and biotite were
559 observed on the MSFRC diffractograms (25°C-Zone 3). As reported by Chaki [31],
560 between 400°C and 600°C, a great increase in the volume of connected voids can be
561 expected in granite aggregates. In addition, the α–β phase transition of quartz (570°C),
562 present in granite, can result in an abrupt increase of more than 1% in the aggregate
563 thermal expansion (between 400°C and 600°C) [32]. Such reversible phase change
564 greatly reduces the compressive strength of concrete after the cooling process [6,33,34].
565 The only studied composites subjected to such a severe condition were the MSFRCs
566 heated up to 600°C. Literature data [28,27] about temperature distribution in cylindrical
567 specimens heated up to 600°C, suggest temperatures of around 500°C for the concrete
568 portion distant 50 mm from the surface (after one hour at the target temperature). In this
569 context it is acceptable to presume that α–β phase transition of quartz occurred only
570 between Zone 1 and 2 in the studied specimens. As reported before, the average tensile
571 strength of the MSFRCs heated up to 600°C was 62.6% lower than that obtained for the

572 reference specimens (25°C). Regarding compressive strength and elastic modulus, the
573 losses were of, respectively, 64.9% and 96.6% (see Table 4).
574 Figure 13 presents correlations of the vertical displacement measurements (δ_P) with the
575 TCOD values obtained in the BCN tests for all studied temperatures. Given the partial
576 fiber decomposition occurred in the Zone 1 and the low strength capacity of the remaining
577 reinforcement at the Zones 2 and 3 of the MSFCR heated up to 400°C, great TCOD values
578 are obtained for small displacement increments right after the cracking formation. In
579 addition, greater penetrations of the steel punch are observed for 400°C and 600°C caused
580 by the crushing of the porous matrix.

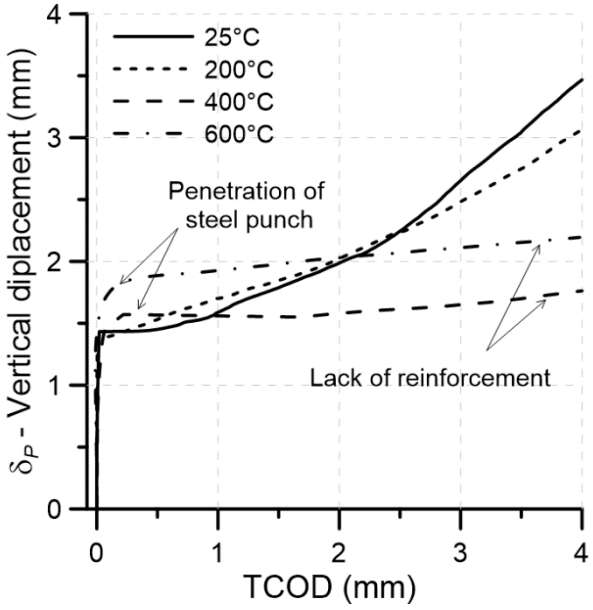

581

582 (Single column fitting image; grayscale)

583 Figure 13 – Correlation between the vertical displacement (δ_P) and the TCOD for the
584 BCN tests performed at room temperature and after heating process up to 200°C, 400°C
585 and 600°C.

586

587 The puncture itself is a feature of the BCN test, however, in the case of residual tests,
588 puncture may result in misleading conclusions, mainly associated with the toughness of

589 the composite. Greater penetrations result in friction between the steel punch and the
590 concrete matrix that may be confused with the bridging effect caused by the fibers.

591 **4. Conclusions**

592 The effect of temperature on the mechanical behavior of the macro-synthetic fiber
593 reinforced concrete was very similar to that known for conventional concrete and that
594 obtained in other studies concerning mechanical strength and elastic modulus. This is a
595 favorable condition in terms of predicting material behavior.

596 The stress-strain curves obtained from the BCN tests demonstrated that the MSFRC
597 gradually loses tensile strength an energy consumption density with increasing
598 temperature. As well as in the case of compressive strength, the ability of the material to
599 bear stresses is significantly reduced from 400°C and above. Such decreases come from
600 the intense decomposition of CSH and AFt along the specimen depth, even in the inner
601 portions of the specimens (i.e.: Zone 3). The temperature of 570°C also represent a critical
602 point since the α–β phase transition of quartz damages the structural integrity of the
603 specimens.

604 The residual tensile strength and elastic modulus of the macro-synthetic fibers were not
605 affected by the temperature up to 100°C. For higher temperatures, however, the
606 reinforcement showed that may lose part of its crystallinity (directly linked to its tensile
607 strength) or even fully decompose, which explain the reduction of the energy
608 consumption density presented by the composite at higher temperatures.

609 The degree of the specimen surface degradation affects the BCN test result in the case of
610 high temperature tests. This effect can be more pronounced for the first crack values given
611 the penetration of the steel punches into the porous matrix. Nevertheless, the gradient of
612 temperature stablished within the specimens may preserve part of the material (i.e.: matrix
613 and fibers), and consequently, the composite post cracking performance.

614 The constitutive model used to determine the stress-strain curves is sensitive to the
615 damage produced in the different MSFRC specimens by the exposure to high
616 temperatures. Therefore, it capable to reproduce the behavior of the composite material
617 after the event of a fire.
618 In general, the most demanding design conditions for precast tunnel segments occur
619 during transient stages (production, storage, transport, installation, etc). In this context,
620 an additional safety margin should exist in the service stage. Although such safety margin
621 would be reduced in the event of a fire, the remaining resistant capacity may be enough
622 to ensure safety in service depending on the temperature reached. The results herein
623 presented may contribute to the definition of parameters that help evaluating such
624 scenario, which should be addressed in future studies.

Funding: This work was supported by the São Paulo Research Foundation (FAPESP) [grant number #2015/25457-9 (Dimas Alan Strauss Rambo)];

Conflicts of interest: none

Acknowledgement: The authors thank Ronaldo dos Anjos for his assistance in editing the images.

631 **References**

[1] J.R. Roesler, S.A. Altoubat, D.A. Lange, K.A. Rieder, G.R. Ulreich, Effect of synthetic fibers on structural behavior of concrete slabs-on-ground, ACI Mater. J. 103 (2006) 3–10.

[2] A.M. Alani, D. Beckett, Mechanical properties of a large scale synthetic fibre reinforced concrete ground slab, Constr. Build. Mater. 41 (2013) 335–344. doi:10.1016/j.conbuildmat.2012.11.043.

[3] A. De La Fuente, R.C. Escariz, A.D. De Figueiredo, A. Aguado, Design of macro-synthetic fibre reinforced concrete pipes, Constr. Build. Mater. 43 (2013) 523–532. doi:10.1016/j.conbuildmat.2013.02.036.

[4] P. Pujadas, A. Blanco, S.H.P. Cavalaro, A. Aguado, S. Grünewald, K. Blom, J.C. Walraven, Plastic fibres as the only reinforcement for flat suspended slabs: Parametric study and design considerations, Constr. Build. Mater. 70 (2014) 88–96. doi:10.1016/j.conbuildmat.2014.07.091.

[5] A. Bentur, S. Mindess, Fibre Reinforced Cementitious Composites, Taylor & Francis Group (2006) 625.

[6] Z. P. Bažant, M. F. Kaplan, Concrete at High Temperatures: Material Properties and Mathematical Models, Longman (1996) 412.

[7] C. Maluk, L. Bisby, G.P. Terrasi, Effects of polypropylene fibre type and dose on the propensity for heat-induced concrete spalling, Eng. Struct. 141 (2017) 584–595. doi:10.1016/j.engstruct.2017.03.058.

[8] P. Sukontasukkul, W. Pomchiengpin, S. Songpiriyakij, Post-crack (or post-peak) flexural response and toughness of fiber reinforced concrete after exposure to high temperature, Constr. Build. Mater. 24 (2010) 1967–1974. doi:10.1016/j.conbuildmat.2010.04.003.

[9] P. Rinaudo, I. Paya-Zaforteza, P.A. Calderón, Improving tunnel resilience against fires: A new methodology based on temperature monitoring, Tunn. Undergr. Sp. Technol. 52 (2016) 71–84. doi:10.1016/j.tust.2015.11.021.

[10] J. Gehandler, H. Ingason, A. Lönnermark, H. Frantzich, M. Strömgren, Performance-based design of road tunnel fire safety: Proposal of new Swedish framework, Case Stud. Fire Saf. 1 (2014) 18–28. doi:10.1016/j.csfs.2014.01.002.

[11] B. Chen, J. Liu, Residual strength of hybrid-fiber-reinforced high-strength concrete after exposure to high temperatures, Cem. Concr. Res. 34 (2004) 1065–1069. doi:10.1016/j.cemconres.2003.11.010

[12] G.F. Peng, W.W. Yang, J. Zhao, Y.F. Liu, S.H. Bian, L.H. Zhao, Explosive spalling and residual mechanical properties of fiber-toughened high-performance concrete subjected to high temperatures, Cem. Concr. Res. 36 (2006) 723–727. doi:10.1016/j.cemconres.2005.12.014.

[13] M. Colombo, M. Di Prisco, R. Felicetti, SFRC exposed to high temperature: Hot vs. residual characterization for thin walled elements, Cem. Concr. Compos. 58 (2015) 81–94. doi:10.1016/j.cemconcomp.2015.01.002.

[14] D. Choumanidis, E. Badogiannis, P. Nomikos, A. Sofianos. Barcelona test for the evaluation of the mechanical properties of single and hybrid FRC, exposed to elevated temperature. Constr. Build. Mater. 138 (2017) 296-305. doi: 10.1016/j.conbuildmat.2017.01.115

[15] UNE 83515: 2010, Hormigones con fibras. Determinación de la resistencia a fisuración, tenacidad y resistencia residual a tracción. Método Barcelona. The Spanish Association for Standardisation, Madrid, 2010.

[16] UNE 83504: 2004, Hormigones con fibras. Fabricación y conservación de probetas para los ensayos de laboratorio. The Spanish Association for Standardisation, Madrid, 2004.

[17] A. Blanco, P. Pujadas, S. Cavalaro, A. De La Fuente, A. Aguado, Constitutive model for fibre reinforced concrete based on the Barcelona test, Cem. Concr. Compos. 53 (2014) 327–340. doi:10.1016/j.cemconcomp.2014.07.017.

[18] fib Model Code 2010, International Federation for Structural Concrete, Lausanne, 2013.

[19] ITA, 2004. Guidelines for structural fire resistance for road tunnels, in: Working Group. doi:10.1016/j.tust.2004.01.001

[21] A. R. Estrada, I. Galobardes, A. D. de Figueiredo. Mechanical Characterization of Synthetic Macrofibres. Materials Research, 19 (2016) 711-720. doi: 10.1590/1980-5373-MR-2015-0680

[20] H.A. Maddah, Polypropylene as a Promising Plastic: A Review, Am. J. Polym. Sci. 6 (2016) 1–11. doi:10.5923/j.ajps.20160601.01.

[21] N.G. MCCRUM, C. P. BUCKLEY, C. B. BUCKNALL. Principles of Polymer Engineering. Second Edition ed. Oxford, New York: Oxford University Press, 1997.

[22] M. Tian, J. Han, H. Zou, H. Tian, H. Wu, Q. She, W. Chen, L. Zhang, Dramatic influence of compatibility on crystallization behavior and morphology of polypropylene in NBR/PP thermoplastic vulcanizates, J. Polym. Res. 19 (2012). doi:10.1007/s10965-011-9745-9.

[23] P. Pujadas, A. Blanco, S.H.P. Cavalaro, A. De La Fuente, A. Aguado, Multidirectional double punch test to assess the post-cracking behaviour and fibre orientation of FRC, Constr. Build. Mater. 58 (2014) 214–224. doi:10.1016/j.conbuildmat.2014.02.023.

[24] A. Blanco, C. Aire, P. Pujadas, S.H.P. Cavalaro, Luong test for the characterization of the shear post-cracking response of fiber reinforced concrete, Constr. Build. Mater. 149 (2017) 207–217. doi:10.1016/j.conbuildmat.2017.05.135.

[25] H.F.W. Taylor, Cement chemistry. 2nd ed., Acad. Press. 20 (1997) 335. doi:10.1016/S0958-9465(98)00023-7.

[26] J.A. Diaz, J.P. Youngblood, Multivariable dependency of thermal shrinkage in highly aligned polypropylene tapes for self-reinforced polymer composites, Compos. Part A Appl. Sci. Manuf. 90 (2016) 771–777. doi:10.1016/j.compositesa.2016.09.004.

[27] L. Phan, Spalling and mechanical properties of high strength concrete at high temperature, in: Concr. Under Sev. Cond. Environ. Load. (CONSEC '07), 2007: pp. 1595–1608. http://fire.nist.gov/bfrlpubs/build07/art019.html.

[28] F.U.A. Shaikh, V. Vimonsatit, Effect of cooling methods on residual compressive strength and cracking behavior of fly ash concretes exposed at elevated temperatures, Fire Mater. 40 (2016) 335–350. doi:10.1002/fam.2276.

[29] M.M. El-Tonsy, Automatic measurement of the absolute CTE of thin polymer samples: I—effect of multiple processing on thermal expansion of polypropylene films, Pol. Test. 23 (2004) 355–360. doi:10.1016/S0142-9418(03)00102-8

[30] G. Odian, Principles of polymerization, 2004. doi:10.1002/047147875X.ch3.

[31] S. Chaki, M. Takarli, W.P. Agbodjan, Influence of thermal damage on physical properties of a granite rock: Porosity, permeability and ultrasonic wave evolutions, Constr. Build. Mater. 22 (2008) 1456–1461. doi:10.1016/j.conbuildmat.2007.04.002.

[32] P. Hartlieb, M. Toifl, F. Kuchar, R. Meisels, T. Antretter, Thermo-physical properties of selected hard rocks and their relation to microwave-assisted comminution, Miner. Eng. 91 (2016) 34–41. doi:10.1016/j.mineng.2015.11.008.

[33] K.D. Hertz, Concrete strength for fire safety design, Mag. Concr. Res. 57 (2005) 445–453. doi:10.1680/macr.2005.57.8.445.

[34] W.D.A. Rickard, G.J.G. Gluth, K. Pistol, In-situ thermo-mechanical testing of fly ash geopolymer concretes made with quartz and expanded clay aggregates. Cem. Concr. Res. 80 (2016) 33–43. doi:10.1016/j.cemconres.2015.11.006